UC Riverside
UC Riverside Previously Published Works

Title

Pathway Specific Unbinding Free Energy Profiles of Ritonavir Dissociation from HIV-1 Protease.

Permalink

https://escholarship.org/uc/item/8jg546cc

Authors

Vig, Emily

Sun, Jianan

Chang, Chia-En

Publication Date

2025-02-09

DOI

10.1021/acs.biochem.4c00560

Peer reviewed

Pathway Specific Unbinding Free Energy Profiles of Ritonavir Dissociation from HIV-1 Protease

Emily Vig[§],
Department of Biochemistry and Molecular Biology, University of California Riverside, Riverside, California 92521, United States

Jianan Sun[§],
Department of Chemistry, University of California Riverside, Riverside, California 92521, United States

Chia-en A. Chang
Department of Chemistry, University of California Riverside, Riverside, California 92521, United States; Department of Chemistry, University of California Riverside, Riverside, California 92521, United States

Abstract

Investigation of protein–drug recognition is key to understanding drug selectivity and binding affinity. In combination, the binding/unbinding free energy landscape and intermolecular interactions can be used to understand drug binding/unbinding mechanisms. This information is vital for the development of drugs with improved efficacy and explanation of mutation effects. This study investigated the dissociation processes of ritonavir unbinding from HIV protease (HIVp). Analyzing unbinding trajectories modeled by accelerated molecular dynamics (MD) simulations, three distinct pathways, pathways A─C, were characterized. Using a reduced dimensionality strategy with the principal component analysis, we carried out short classical MD runs with explicit water to sample local fluctuation during ritonavir dissociation and applied the milestoning theory to construct an unbinding free energy landscape. We found that each pathway showed similar values of binding free energy, albeit pathway A accounts for over 50% of dissociation trajectories. Interestingly, residue–residue correlation network analysis showed that in pathway A, a broad correlation network outside the flap region governs protein motions during ritonavir unbinding, which includes residues with reported mutation effects. However, the other two pathways showed limited correlation networks where no reported mutated residues were involved, explaining the favorability of pathway A. Guided by the free energy profile, we investigated each energy barrier and minimum, demonstrating that hydrogen bonding governed

movement of the flap regions, directly impacting the calculated energy. Our study provided a new strategy to estimate ligand binding free energy and demonstrated the importance of the transient interactions during ligand–protein dissociation pathways in understanding drug unbinding.

Graphical Abstract
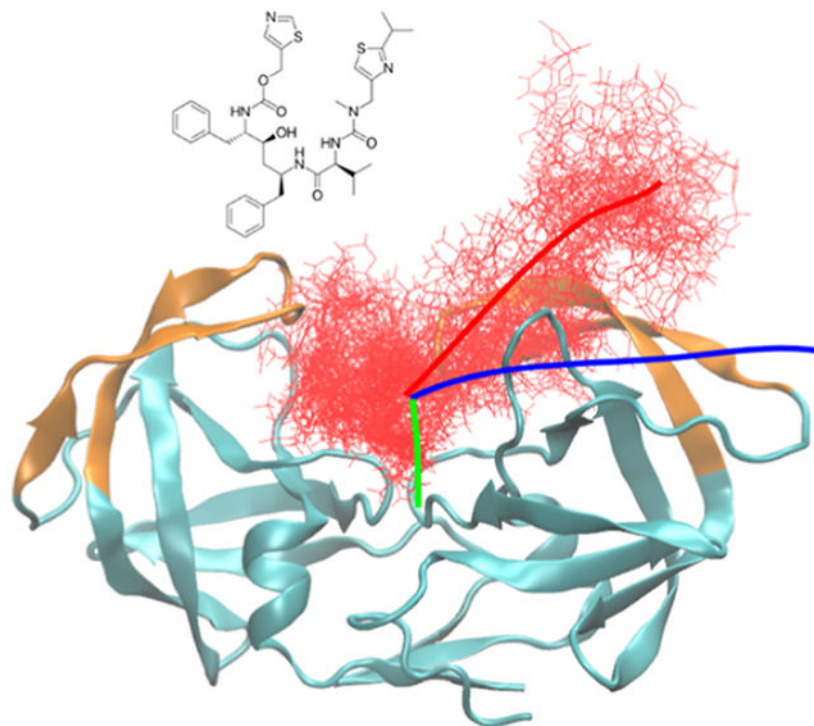
INTRODUCTION

Drug development relies heavily on a thorough understanding of how proteins and drugs interact.[1] Knowledge of protein–drug interactions, both in bound and transient states, enables researchers to strategically develop drugs, thus improving their ability to selectively bind to proteins of interest.[2-4] The dynamic nature of molecular interactions results in a complex environment in which many transient states occur over the course of drug binding and dissociation.[5] These transient states arise within an energy landscape in which different conformations correspond to different energy states. Various unbinding pathways often emerge as the system explores these energy minima and transition states during the unbinding process.[6] Protein–drug interactions often differ between binding and unbinding pathways that contribute to their binding affinity; however, these intermediate processes are left unstudied by traditional approaches. Further, residues mutations, both in or outside the binding pocket, may induce structural and dynamic changes of proteins, which may have a substantial influence on protein–ligand interactions which impact drug potency, efficacy, and selectivity.[7,8] Because of this, thoroughly investigating protein–drug interactions can provide explanations for drug resistance associated with protein mutations, both natural and induced.

Understanding the thermodynamic and kinetic properties of drug binding and unbinding is of fundamental importance for determining the efficacy of a drug.[9] The dissociation rate constant, $1/k_{off}$, can be used directly to estimate the drug residence time.[10] Residence time is a key indicator used in accessing drug efficacy, as drugs are only effective when bound to their respective target.[11] Experiments measured thermodynamic and kinetic properties of protein–drug binding such as rate constants (k_{on} and k_{off}) and binding affinity (G). While these important values are used to guide drug design, solely the measurements do not interpret and illustrate the complete picture of structure-kinetics and/or structure–affinity relationships in protein–ligand systems. To achieve a complete and thorough understanding of drug binding, computational methods can be used to illustrate and connect structural interactions with thermodynamics, kinetics, and mechanisms of molecular processes. With these measured properties we can strategically plan a drug development process to improve both specificity and efficiency. This is of extreme interest in current drug development in which druggable targets have been identified, including human immunodeficiency virus (HIV).

HIV is a potentially life-threatening virus that attacks the human immune system and, when left untreated, results in acquired immunodeficiency syndrome (AIDS). A few viral proteins have been utilized for AIDS treatments, such as HIV-1 protease (HIVp).[12] However, as the viral proteins constantly mutate, the development of drugs to kill HIV has proved difficult. HIVp is a symmetrical homodimeric protein responsible for the cleavage of premature viral proteins.[13] This cleavage is responsible for the formation of mature, infectious HIV particles.[14] HIVp serves as a prominent model system in scientific research and drug development[15] (Figure 1A). The well-defined three-dimensional structure of HIVp allows insight into its molecular functions, facilitating the modeling and optimization of inhibitors in rational drug design.[16] Protease inhibitors, which comprise a class of antiretroviral drugs, work by obstructing HIVp and inhibiting its function. One unique feature of HIVp is the well-documented characteristic flap movement, opening and closing, which serves as a gate to govern natural substrate and drug binding/unbinding.[17,18] Understanding the flap movement is crucial for designing effective inhibitors.[19] Many HIVp inhibitors work by binding to the enzyme's active site and stabilizing the closed state.[20-22] This closed state prevents the flaps from opening, thus inhibiting the enzyme's catalytic activity. This prevents the formation of infectious viral segments, thereby limiting the progression of HIV infection. Studying the dynamics of flap movement and different drug binding/unbinding pathways with the flap dynamics provides insights into the molecular mechanisms of HIVp inhibitor binding and aids in better developing antiretroviral drugs incorporating this dynamic process.[23] The mechanism of action of these HIVp inhibitors serves as a model for understanding enzyme inhibition, contributing to a broader knowledge applicable to other enzymatic systems.

Ritonavir is a common HIVp inhibitor that is used in the treatment of HIV[24] (Figure 1B). Ritonavir noncovalently binds to HIVp and stabilizes the closed state. Experimental techniques (i.e., X-ray crystallography) determine 3-dimension structures that allow observation of ritonavir bound to HIVp.[25] However, crystal structures lack movement and do not give insights into all of the interactions that occur during the unbinding of ritonavir from HIVp. This is particularly important when flap mobility is key in drug-unbinding. While

nuclear magnetic resonance (NMR) spectroscopy can provide quantitative information on protein dynamics, NMR has limitations in revealing all atomistic details during drug binding/unbinding. Understanding these dynamic interactions is crucial, as HIVp mutations, which affect flap mobility, have been shown to increase resistance to ritonavir.[26] Insights into ritonavir's dynamic interactions with HIVp may help to explain this resistance.

Molecular dynamics (MD) simulations model movements of protein–drug complexes over time, providing insights into the interactions and structural changes associated with drug association/dissociation.[27] MD allows for the visualization of unbinding pathways and can handle large, complex systems, making it ideal for understanding dynamic processes and resistance mechanisms. In conventional molecular dynamics (cMD) simulations, the time that it takes for a drug to dissociate from a protein can vary greatly. For strong binders, dissociation might take milliseconds to hours. As cMD typically only simulates nanoseconds to microseconds of realtime dynamics, observing spontaneous dissociation within this period is highly unlikely unless additional techniques are used to speed up the process. Enhanced sampling techniques have been widely used to investigate ligand binding kinetics.[28] For example, using accelerated molecular dynamics (aMD) has allowed efficient conformational sampling of HIVp by reducing energy barriers which resultingly increases the occurrence of rare events.[29,30] In combination with a reseeding approach, aMD can be used to collectively study rare dissociation events in great numbers. Earlier studies using this approach have shown that ritonavir dissociates from the binding pocket via three distinct pathways.[31] Though past simulations have shown the presence of multiple pathways, additional analysis and constructing a ligand unbinding free energy landscape further provide quantitative data to understand protein–drug recognition and the probability differences between each pathway. Popular analyses such as molecular mechanics Poisson–Boltzmann surface area (MM-PBSA) provide insights into molecular interaction energy and solvation effects.[32] However, changes of entropy and free energy during ligand binding/unbinding, the vital assessment of molecular flexibility, are difficult to calculate via traditional techniques. As HIVp is known to function largely through flap movements, accurately describing protein flexibility is crucial in fully understanding ligand binding and protein function.

A key metric for understanding the thermodynamics of the complex is the free energy profile, also termed the potential of mean force (PMF). Here the PMF refers to the free energy of a system as a function of a defined coordinate. It is commonly seen for ligands to move back and forth in the binding pocket, as is the case with ritonavir (Figure S1). Therefore, providing a defined coordinate which can accurately describe the molecular movement during drug unbinding is not straightforward. For example, the use of a simple center of mass distance or root-mean-square deviation (rmsd) of ligand position may not be adequate to depict ligand binding or unbinding. As a result, reduced dimensionality using principal component analysis has been utilized to better define a ligand unbinding coordinate.[33]

In this study, we calculated the free energy profile for unbinding of ritonavir from HIVp. We investigated 3 major unbinding pathways and used the binding kinetics toolkit (BKiT) package to define the ritonavir unbinding coordinate and construct PMF using many short cMD and the milestoning theory.[34,35] The exact drug–protein interactions from local energy

minima are of extreme interest, as they would affect drug-binding kinetics, even though the absolute binding free energy is the same despite the unique unbinding pathways. Protein–drug conformations existing at minima stabilize the HIVp–ritonavir complex. By connecting local free energy minima and barriers to key unbinding events, we can verify the free energy profiles and explain how hydrogen bonding in flap regions impacts free energy. Energy wells are directly attributed to hydrogen bonding between ritonavir and HIVp, stabilizing the bound complex. Further, side chain correlation studies provide insight into total protein movement and cohesiveness unique to each of the three pathways. Understanding protein movement and ligand–protein interactions at transient states can help us optimize drugs with desired kinetic properties[36,37] as well as provide insight into the cause of mutation-related drug resistance.

MATERIALS/EXPERIMENTAL DETAILS

Molecular Systems.

Ritonavir–HIVp dissociation trajectories sampled by aMD were taken from published work that used Amber14SB for protein and GAFF for ligand.[31] The initial frame of aMD was taken from 100 ns cMD runs, which used the protein data bank entry 1HXW as the initial bound state, with a single protonation state applied for Asp25. AMD allows for the sampling of rare dissociation events by adding a continuous non-negative bias or "boost" potential. Both dihedral and total potential energy boosts were applied. Boost factors were calculated based on 100 ns bound state ritonavir–HIVp cMD simulations. Reseeding was used to generate multiple MD simulation production runs from one initial conformation. AMD, when combined with reseeding, results in the capturing of many ritonavir unbinding events. In order to better sample these unbinding events, we selected frames from the aMD dissociation trajectories as the initial frames for short MD runs. Initial frames for short MD runs were taken every 100 ps for the majority of the simulation. As ligand leaves the binding pocket, we decrease the interval of initial frame selection to once every 20 ps to better cover the PC space. Initial frames varied between pathways to account for differences in the simulation length. The breakdown of initial frames is detailed in Table S1. We ran 10 replicas of short MD runs for each initial frame. Explicit solvent was used. All short MD runs were 100 ps long unbiased cMD with the TIP3P water model, Amber14SB for protein, and GAFF for ritonavir at 298 K. Frames in short MD runs were saved every 100 fs. By using many short MD runs, we are able to (1) sample transitions between unbinding indexes and (2) validate proposed dissociation pathways.

Constructing the Unbinding Free Energy Profile.

Defining Unbinding Coordinates.—To project high dimensional trajectories into low dimensional spaces, Cartesian coordinates are taken from aMD and stored in a matrix consisting of the x,y,z coordinates of each α carbon of HIVp and each heavy atom of ritonavir. This matrix is then projected onto the principal component (PC) space. Only the first two PCs (PC1 and PC2) are generated. PC space encapsulates the key motions of ritonavir into a smaller subset of the principal components. This results in a series of positions that represent the primary motions ritonavir undergoes during dissociation from HIVp. A score plot is made of PC1 vs PC2 and a smooth path is generated by taking

a continual average of frames before and after 100 steps of each frame. Loops are then removed from the smoothed path, and milestones are placed with a width of 4 Å. Each milestone represents an unbinding index, a key position of ritonavir during dissociation from HIVp.

Defining Representative Frames.—Representative clusters for the unbinding index are then defined as projected frames that fall within 1.5 Å of a milestone. For any given unbinding index, we keep at most 10 configurations that fall closest to the milestone. These frames are saved for the validation of unbinding trends associated with each milestone. A trajectory can then be created by using one representative frame for each milestone. For milestones with multiple frames per representative cluster, we selected the frame nearest to the average in the PC1/PC2 space as the representative frame. For milestones with no representative clusters, we use a representative frame from the neighboring milestone.

Construction of the Transition Matrix.—Transitions between the unbinding indexes are computed by analyzing the system behavior in numerous short MDs. We provide two methods of constructing transition matrix, PC based or ligand rmsd based. For the PC based method, unbinding indexes are found, as previously described. The system movement in each short MD is examined and judged to see whether it crossed any two consecutive unbinding indexes. If a transition occurs, two neighbor unbinding indexes and frames are recorded to compute the time needed in such a transition. BKiT counts numerous transitions and computes the average lifetime (τ_i) and its standard deviation ($\sigma_{\tau,i}$) of each transition. This data then is used to construct a transition matrix, which quantifies the probability of transition in or out of each unbinding index. The ligand rmsd based method uses the same protocol for constructing the transition matrix instead using ligand rmsd as initial unbinding indexes.

Constructing the Unbinding Free Energy Profile.—The free energy profile, also termed the PMF, provides quantitative free energy values using the unbinding index as a reaction coordinate. This allows us to examine energy trends relative to each stage of ritonavir's dissociation. Free energy of each unbinding index can be calculated by $F = -K_\mathrm{B}T \; \ln(q_i t_i)$ where q_i is the stationary flux of each unbinding index (i) and t_i is the averaged lifetime of unbinding index (i). Stationary flux quantifies the number of transitions into any given unbinding index per unit time as computed from the transition matrix. Bkit computes the stationary flux by solving the eigenvalues of the transition kernel. Eigenvalues equal to 1, the highest possible value, represent the stationary flux. The binding free energy is estimated as the difference of the lowest energy (bound state) and highest energy (unbound state or max energy barrier) on the free energy landscape. The mean first passage time (MFPT) of index n can be estimated by $\mathrm{MFPT} = \sum q_i t_i \, / \, q_n$, where residence time is estimated when the index *n* shows that the ligand already unbinds from the pocket.

Examining Ligand–Protein Interactions and Stability Factors.

Hydrogen Bond Analysis.—The unbinding free energy is largely determined by interactions within the protein. For instance, each hydrogen bond between the ligand and protein may contribute up to a few kcal/mol to interaction energy.[38] To hydrolyze

the peptide bond in premature protein, Asp25/124 establishes hydrogen bonding with the peptide backbone in the substrate, whereas Ile50/149 stabilizes the substrate with a water bridge.[39] To better understand which residues may form H-bonds with ritonavir during ligand dissociation, we analyzed and plotted H-bond versus time by using the CPPTRAJ program.[40] The criteria for H-bonding are (1) the distance between donor D and acceptor A < 3 Å, and (2) the D-H-A angle, where H is the shared hydrogen, at least 150°. Hydrogen bonds were also collected using the VMD hydrogen bond plug-in, following the same parameters.

Pairwise Side Chain Correlation.—Side chain correlation values were measured using T-Analyst.[41] The Pearson correlation formula was used to compute the pairwise correlations. To ensure accuracy and avoid computational errors arising from discontinuity margins (± 180 or $360°/0°$), we transformed the side-chain rotation angles into Cartesian coordinates using eqs 1-3.

$$r_{xy} = \frac{\sum_{i=1}^{n}(x_i - \bar{x})(y_i - \bar{y})}{\sqrt{\sum_{i=1}^{n}(x_i - \bar{x})^2}\sqrt{\sum_{i=1}^{n}(y_i - \bar{y})^2}}$$

(1)

$$\bar{x} = \arctan\left(\frac{\sin(x_1) + \sin(x_2) + \ldots + \sin(x_n)}{\cos(x_1) + \cos(x_2) + \ldots + \cos(x_n)}\right)$$

(2)

$$x_i - \bar{x} = \arctan\left(\frac{\sin(x_i)\cos(\bar{x}) - \sin(\bar{x})\cos(x_i)}{\cos(x_i)\cos(\bar{x}) + \sin(x_i)\sin(\bar{x})}\right)$$

(3)

r_{xy}: dihedral Pearson correlation, $\bar{x}$: mean of dihedral angles, x_i: side chain dihedral angles.

Residues that shared a correlation value above 0.50 were labeled positively correlated with negatively correlated values falling below −0.50. A positive correlation between two side chains suggests that they rotate similarly during MD simulation. As tail regions show high movement, there are increased odds of capturing correlation by chance. For this reason, correlation pairs including tail regions have been negated. For residues in which multiple dihedrals showed correlation, the dihedral with the highest correlation value was reported.

RESULTS AND DISCUSSION

This section begins by reporting ritonavir unbinding free energy landscape for distinct unbinding pathways sampled by aMD runs.[31] Pathway A describes unbinding between the flap region and the loop region. Pathway B describes surface-level diffusion through the flap region. Pathway C describes surface-level diffusion through the interface region. Of these studies, pathway A accounted for over 50% of dissociation trajectories. We showed

that ritonavir's navigation through HIVp in each pathway and drug–protein interactions associated with each pathway differ greatly. We used two unbinding coordinates to present the unbinding index for constructing PMF. The investigation of residue–residue correlation and the implications of mutation effects are also discussed.

Computed Unbinding Free Energy Landscape.

Using PC Space to Compute Free Energy Landscape and Residence Time.—

Using a coordinate to precisely describe ligand unbinding from the protein pocket is crucial in PMF calculations. Only when the unbinding coordinate can be reasonably described, which include key movements of protein side chains and ligand functional groups, the free energy barriers and minima shown in the computed free energy landscape can accurately associate with ligand dissociation processes and explain binding kinetics. As demonstrated in Figure S3, we first performed principal component analysis (PCA) and project the Cartesian coordinate representation with high-dimensional ligand–protein motions ($3N$-6 degrees of freedom, where N is the number of atoms) to only two-dimension (2D) space using the first 2 PC modes (degrees of freedom). We used the BKiT package to assign milestones in the 2D-PC space, and construct PMF using various short 100 ps classical MD runs.

As illustrated in Figure 2, the calculations revealed a rugged ritonavir unbinding free energy landscape, where the free energy barriers and minima shown in the landscape associate with important molecular movements, as discussed in the next subsection. Unbinding free energies and residence time of ritonavir–HIVp were also approximated from the PMF (Table 1, left column). PC modes represent fundamental motions during ritonavir dissociation, where pathways A and B share similar unbinding free energy values, −9.4 and −9.5 kcal/mol, respectively. Pathway C is less energetically favorable, with an unbinding free energy of −6.1 kcal/mol. Pathways A and B demonstrate a gradual increase in energy as the unbinding progresses (Figure 2A,B), while pathway C shows a large and shallow free energy well during ligand unbinding (Figure 2C). It should be mentioned that the free energy profiles for each pathway lack a clear plateau which would typically be expected.[42,43] This is due to incomplete sampling of the unbound state. As the interaction energy is close to zero, a complete sampling of the free energy barrier would require thorough sampling of surface interactions to account for entropic penalty. This level of sampling is computationally expensive but offers little additional insight into drug discovery. For example, under our current sampling conditions, it is estimated to take about 92 h with 10 nodes (1GPU + 1CPU) running simultaneously to complete short cMDs for all three dissociation trajectories. Capturing the unbound state would greatly increase this run time. As we focus primarily on local free energy minimia and barriers and mechanistic insights of unbinding prior to the fully unbound state, our margin of error of total unbinding free energy falls within an acceptable range of experimental values. PMF calculations are relatively inexpensive, taking approximately one h per pathway on a single GPU to construct a transition matrix, making this a practical method for computation of local energy trends.

Using Ligand rmsd to Compute Free Energy Landscape and Residence Time.
—While the PMF using the 2D PC space to present the unbinding coordinate provides

valuable insights into HIVp and ritonavir movement during ritonavir unbinding, the absolute binding free energies from all 3 pathways were underestimated, compared with the experimental binding free energy of ~−13.7 kcal/mol. The respective residence times also differed from the experimental value of 463 s. As detailed in a published work, the differences between the computed and experimental values mainly came from skipping data points when counting transitions between milestone indexes presented by straight lines in the 2D space[44] (Figure S7). In addition, missing coverage of molecular motions using the first 2 PC modes. The combined coverage of the first 2 PC modes for ritonavir unbinding from HIVp under pathway A was 56%, where 44% of the motions were not considered in the 2D space. Pathways B and C had 69.8% and 60.9% coverage, respectively. Therefore, to avoid skipping data points when using a line in the 2D space, we used ligand rmsd to present ritonavir unbinding with 0.1 Å intervals to present milestones. This one-dimensional (1D) milestone index can ensure that every transition between two adjacent milestones is counted, and no data point is skipped. The computed binding free energy with the 1D milestone index under pathway A, B, and C are −14.1, −15.4, and −14.9 kcal/mol, respectively (Table 1, middle column), which are in good agreement with experimental measurement. The computed drug residence times for ritonavir dissociation from HIV protease under pathways A, B, and C are 2.5 41.6, and 29.6 s, respectively, which are in the ballpark of experimental residence time, ~463 s. It is important to note that experimental residence times are an ensemble, while the computational residence time for each pathway is constructed from one pathway. This leads to an inherent degree of error, particularly for pathways that happened rarely. Once again, due to the low cost of these calculations and the complexity in estimating drug residence times, the moderate accuracy of our residence time calculations provides useful insight. While use of 1D to present milestones can accurately reproduce experimental binding free energy and residence time, using ligand rmsd cannot accurately describe HIVp and ritonavir motions during ligand unbinding (Figures S1 and S2). Ritonavir exhibits a back-and-forth motion during dissociation. By this, we mean that ritonavir may away from a stable local free energy minimum slightly before returning to its previous position. This is not atypical of drugs during dissociation. rmsd does not provide a spatial component as it only measures absolute distance. Because of this motion, several different conformations may all have the same rmsd value (Figure 3). Using the rmsd to create a free energy landscape results in a plot without clear peaks, leaving us unable to further evaluate the mechanism using local minima and maxima. Using PCA allows us to estimate the relative energy, although the total unbinding free energy was underestimated. Nevertheless, this correction validates that the error sources came from the use of milestones presented by lines in the 2D PC space, which inevitably skip transition counts.

Thermodynamic Investigation of Free Energy Landscape.—By examining the free energy landscape, we are able to illustrate the relative stability of different HIVp–ritonavir conformations and provide insights into how and why the transitions occur between the free energy minima and barriers. Here we aim to examine conformations associated with these energy minima and barriers to learn the governing key interactions that occur during ritonavir dissociation. We showed that these interactions are different between dissociation pathways and also influence the overall movement of HIVp. Further, by being able to

connect energy data to existing interactions, we validate both the unbinding pathway and the free energy landscape.

Free Energy Landscpe under Pathway A.—The unbinding free energy landscape identifies three major energy wells and three major energy barriers over the course of ritonavir's dissociation from HIVp via pathway A (Figure 4). The computed free energy landscape correctly captured the interactions of the crystal-bound state at energy minimum A (Figure 5A). Upon visual analysis, it was concluded that the computed free energy landscape can correctly capture the crystal bound state. By visualizing ritonavir–HIVp interactions at energy minima A, we found hydrogen bonds between ritonavir and Asp25 and Asp 29, in addition to pi-stacking between ritonavir and Arg107. As the system progressed, interactions between ritonavir and HIVp were broken, giving us energy barrier B (Figure 5B). As ritonavir approaches Thr 80, a strong hydrogen bond of 1.8 Å between the hydroxyl groups of ritonavir and Thr 80 was formed, which further attracted ritonavir to the loop region of Thr 80 (Figure 5C). More interactions were followed by such hydrogen bonds. Gly 150 and Ile 149 formed hydrogen bonds with ritonavir as well. Nonpolar attraction between Ile 146 and ritonavir was also observed. Flap regions of HIVp opened, exposed ritonavir to solvent, and reduced contact with ritonavir, giving energy barrier D (Figure 5D). Nonpolar attraction was the major interaction between ritonavir and HIVp. As ritonavir keeps moving to the left side of HIVp, the flap region on the right side closed, resulting in a slightly lower energy barrier compared to barrier D (Figure 5E). Once ritonavir moved to the gap between flap and loop region, a local energy minimum was observed at energy well F (Figure 5F). As ritonavir kept moving along unbinding pathway A, it temporarily formed a hydrogen bond with Lys 154, resulting in a tiny energy minimum at G (Figure 4G), prior to ritonavir's complete dissociation.

Free Energy Landscape under Pathway B.—We further constructed the free energy landscape of ritonavir unbinding from HIVp under pathway B (Figure 6). Once again, the computed free energy landscape correctly captured the interactions of the crystal bound state at energy minimum A (Figure 7A). These hydrogen bonds were broken at energy barrier B (Figure 7B). Since pathway B involves ligand diffusion on the flap region, minimal interactions between ritonavir and the loop region were observed. At energy minimum C, ritonavir formed hydrogen bond with Asp 128, Gly 51 and Gly 148 (Figure 7C). Energy well D was observed with a hydrogen bond between ritonavir and Asp 128, Ile 149 (Figure 7D). As flap regions opened widely and exposed ritonavir to solvent, reduced contact between ritonavir and HIVp and broken hydrogen bonds, a steep energy barrier showed up from D to E, where minimal contact between ritonavir and HIVp was presented at energy barrier E (Figure 7E). As ritonavir moved along the flap region, it encountered Lys 142 and formed a transient hydrogen bond, giving a small energy well, F (Figure 7F).

Free Energy Landscape under Pathway C.—We further examine the free energy landscape of ritonavir unbinding from HIVp under pathway C (Figure 8). The computed free energy landscape correctly captured the interactions of the cocrystal bound state of ritonavir–HIVp (Figure 9A) and the breaking of these hydrogen bonds at energy barrier B (Figure 9B). At the local energy minimum C, ritonavir was mostly attached to the flap

region with hydrogen bonds to Ile 50, Ile 149, and Gly 151 (Figure 9C). More interactions between ritonavir and interface region of HIVp were observed. At the energy well, D. Ritonavir left the flap region and started contacting Arg 8 with two hydrogen bonds, plus hydrogen bonds with Asp 129 (Figure 9D). As ritonavir kept moving toward the interface region, the attraction between ritonavir and Arg 8 grew strong. Three hydrogen bonds were observed between ritonavir and Arg 8 at energy well E (Figure 9E).

Insights provided from Free Energy Plot.—Energy barriers and wells were successfully attributed to particular protein–ligand interactions, validating the free energy plot specific to each dissociation pathway. These interactions contribute highly to the overall unbinding free energy. Hydrogen bonding was seen to have a large impact on movement in the flap region. However, visual analysis of protein–ligand interactions did not account for the discrepancy in the occurrence between pathway A and the other two pathways. It is likely that an additional component, separate from unbinding energy, is impacting the dissociation of ritonavir from HIVp.

Analysis of Pathway-Specific Side-Chain Correlation.—Mutation studies have shown that single mutations are not impactful on HIVp affinity for substrate, however mutation combinations result in drug resistance.[45] This indicates that single residue studies are not sufficient on their own to understand the ways in which ritonavir can dissociate from HIVp. In combination with the previous single residue studies, we ran a side-chain correlation analysis specific to each of the three pathways. This gives insight into the cohesiveness of the protein in binding to ritonavir. Pathway A exhibited an extensive network of highly correlated residues (Table 2).

These residues had high coverage across the majority protein and were not localized to any singular region, although they were primarily absent in flap regions (Figure 10). Higher amounts of correlated residues were found on the side of HIVp in which ritonavir dissociates along in pathway A. Correlation was demonstrated in mirror loop residues ASN83 and ASN182, indicating symmetric loop movement during ritonavir dissociation. Pathway A demonstrates a highly correlated protein that arranges side-chain movements to interact with ritonavir. The flap regions move according to single residue conflicts and are predominantly governed by hydrogen bonding as it relates to the PMF. However, in pathway A, the rest of the protein exhibits organized motion that helps to shape HIVp and stabilize transient states of ritonavir. This correlation network cannot be predicted using free energy alone. These findings are supported by known resistance data, as residues appearing in the correlation network, ILE84 and Val131, are known to have less favorable interactions in drug resistant strains of HIVp.[45] It is worth noting that when the correlation threshold is lowered below |0.5|, this correlation network is far more expansive and encompasses more known resistance residues.

Pathway B exhibited a less extensive network of highly correlated residues (Table 3). These residues were localized primarily to the interface region and once again were absent in the flap regions (Figure 11). Pathway C lacked a correlation network. Only two residue pairs in pathway C demonstrated a high positive correlation. Pathway c was absent of negatively correlated residues (Table 3).

These residues did not follow any clear pattern or localization and appear random in nature (Figure 12). Neither pathway B nor pathway C had a correlation network involving any residues known to impact drug resistance. Single residues give some insight into the total energy of each dissociation pathway; however, the exceptionally cohesive motion of the protease seems to be the major contributor to pathway A being favored.

CONCLUSIONS

Due to increasing drug resistance from protein mutations, it is increasingly challenging to develop drugs with high efficacy when a protein target mutates. Considering drug binding kinetics by examining the drug binding/unbinding pathways reveals transient states during drug binding/unbinding, which provide a more complete picture of molecular recognition and understanding of mutation effects of distal sites. While many protein systems demonstrate a single channel for ligand binding/unbinding, HIVp has highly flexible flap regions to allow ligand binding/unbinding via different pathways. As a result, examining one single pathway is insufficient to understand drug unbinding. This study therefore investigated different unbinding pathways in detail to uncover key transient states and residues of interest. By combining this with side chain correlation, we uncovered new information on the motion of HIVp as ritonavir dissociates. Our study shows that the computed free energy landscape captures detailed ligand–protein interactions during ligand unbinding using the 2D PC space to define unbinding coordinates and milestones. However, the computed absolute binding free energy and residence time were obtained with moderate accuracy. We also used ligand rmsd as unbinding coordinates, and use of the 1D milestones resulted in accurate absolute binding free energy and drug residence time compared with experimental measurements. Combining these two approaches, we validated our sampled unbinding pathways and demonstrated key interactions that brought about free energy barriers and minima during ritonavir dissociation.

Ritonavir–HIVp interactions, particularly those in the flap region, show that hydrogen bonding contributes significantly to the free energy and governs dissociation of ritonavir from HIVp. These interactions can be directly tied to the unbinding free energy plot in each of the three pathways. However, the studies of ritonavir–HIVp interactions are insufficient to explain the low occurrence of pathway B and pathway C in comparison to pathway A, considering the similarity in the unbinding free energy between the pathways. We therefore carried out side-chain correlation to find the residue–residue interaction network, which is not directly visible in the energy profile. Pathway A exhibits a remarkably large residue correlation in the protease itself, allowing HIVp to adjust intramolecular interactions to better accommodate ritonavir to form hydrogen bonds during ligand dissociation and lead to the most popular unbinding pathway. The correlation analysis disclosed these highly correlated residues in pathway A, which include ILE84 and Val131 reported in mutations and drug resistance. When the residues mutated, the residue correlation network was altered, leading to less stable intermediate states that accelerate drug dissociation. This study explains how the distal sites may affect the drug binding affinity. As the protein most commonly works via a wide-scale correlation network, we also demonstrated that considering single residue-drug contacts is not enough in understanding drug unbinding processes. This explains why multiple mutations need to happen simultaneously to cause

drug resistance to ritonavir. Our study also explains that when mutations occur outside of flap regions, though not directly affecting drug-HIVp binding in the catalytic pocket, it may disrupt the correlation network of HIVp and facilitate the dissociation of ritonavir. These mutation effects would be difficult to predict using thermodynamic data alone. Based on the results of this study, protein correlation may be used as a factor in predicting ligand–protein binding kinetics and specificity. If a ligand–protein system has a widespread correlation network, it may suggest that it can better stabilize transient states, thus making the ligand an ideal inhibitor with a high residence time.

Supplementary Material

Refer to Web version on PubMed Central for supplementary material.

ACKNOWLEDGMENTS

Data Availability Statement

All computational data and input files are available at 10.5281/zenodo.14510545.

REFERENCES

(1). Protein-Ligand Interactions and Drug Design; Ballante F, Ed.; Springer US, 2021; Vol. 2266

(2). Bernetti M; Masetti M; Rocchia W; Cavalli A Kinetics of Drug Binding and Residence Time. Annu. Rev. Phys. Chem 2019, 70, 143–171. [PubMed: 30786217]

(3). Conflitti P; Raniolo S; Limongelli V Perspectives on Ligand/Protein Binding Kinetics Simulations: Force Fields, Machine Learning, Sampling, and User-Friendliness. J. Chem. Theory Comput 2023, 19 (18), 6047–6061. [PubMed: 37656199]

(4). Wong CF 15 Years of molecular simulation of drug-binding kinetics. Expert Opin Drug Discov. 2023, 18 (12), 1333–1348. [PubMed: 37789731]

(5). Hammes G. Mechanism of Enzyme Catalysis. Nature 1964, 204, 342–343. [PubMed: 14228866]

(6). Rydzewski J; Valsson O Finding multiple reaction pathways of ligand unbinding. J. Chem. Phys 2019, 150 (22), 221101. [PubMed: 31202231]

(7). Wang W; Kollman PA Computational study of protein specificity: The molecular basis of HIV-1 protease drug resistance. Proc. Natl. Acad. Sci. U.S.A 2001, 98, 14937–14942. [PubMed: 11752442]

(8). Bastys T; Gapsys V; Walter H; Heger E; Doncheva NT; Kaiser R; de Groot BL; Kalinina O.v. Non-active site mutants of HIV-1 protease influence resistance and sensitisation towards protease inhibitors. Retrovirology 2020, 17 (1), 13. [PubMed: 32430025]

(9). Liu W; Jiang J; Lin Y; You Q; Wang L Insight into Thermodynamic and Kinetic Profiles in Small-Molecule Optimization. J. Med. Chem 2022, 65 (16), 10809–10847. [PubMed: 35969687]

(10). Nelson DL; Cox MM Lehninger Principles of Biochemistry, 7th ed; Freeman WH, 2017.

(11). Tonge PJ Drug–Target Kinetics in Drug Discovery. ACS Chem. Neurosci 2018, 9 (1), 29–39. [PubMed: 28640596]

(12). Friedman SH; Decamp DL; Sijbesma RP; Srdanov G; Wudl F; Kenyon GL Inhibition of the HIV-1 Protease by Fullerene Derivatives: Model Building Studies and Experimental Verification. Am. Chem. Soc 1993, 115, 6506–6509.

(13). Freed EO HIV-1 assembly, release and maturation. Nat. Rev. Microbiol 2015, 13 (8), 484–496. [PubMed: 26119571]

(14). Weber IT; Wang YF; Harrison RW HIV Protease: Historical Perspective and Current Research. Viruses 2021, 13 (5), 839. [PubMed: 34066370]

(15). Huang S; Zou X Efficient molecular docking of NMR structures: Application to HIV-1 protease. Protein Sci. 2007, 16 (1), 43–51. [PubMed: 17123961]

(16). Lee VS; Nimmanpipug P; Aruksakunwong O; Promsri S; Sompornpisut P; Hannongbua S Structural analysis of lead fullerene-based inhibitor bound to human immunodeficiency virus type 1 protease in solution from molecular dynamics simulations. J. Mol. Graph 2007, 26 (2), 558–570.

(17). Deng NJ; Zheng W; Gallicchio E; Levy RM Insights into the dynamics of HIV-1 protease: A kinetic network model constructed from atomistic simulations. J. Am. Chem. Soc 2011, 133 (24), 9387–9394. [PubMed: 21561098]

(18). Kang M; Roberts C; Cheng Y; Chang CA Gating and Intermolecular Interactions in Ligand-Protein Association: Coarse-Grained Modeling of HIV-1 Protease. J. Chem. Theory Comput 2011, 7 (10), 3438–3446. [PubMed: 26598172]

(19). Galiano L; Ding F; Veloro AM; Blackburn ME; Simmerling C; Fanucci GE Drug pressure selected mutations in HIV-1 protease alter flap conformations. J. Am. Chem. Soc 2009, 131 (2), 430–431. [PubMed: 19140783]

(20). Weber IT; Wang Y-F; Harrison RW HIV Protease: Historical Perspective and Current Research. Viruses 2021, 13 (5), 839. [PubMed: 34066370]

(21). Singh G; Senapati S Molecular Dynamics Simulations of Ligand-Induced Flap Closing in HIV-1 Protease Approach X-ray Resolution: Establishing the Role of Bound Water in the Flap Closing Mechanism. Biochemistry 2008, 47 (40), 10657–10664. [PubMed: 18785756]

(22). Shabanpour Y; Sajjadi S; Behmard E; Abdolmaleki P; Keihan AH The structural, dynamic, and thermodynamic basis of darunavir resistance of a heavily mutated HIV-1 protease using molecular dynamics simulation. Front. mol. biosci 2022, 9, 927373. [PubMed: 36046605]

(23). Hornak V; Okur A; Rizzo RC; Simmerling C HIV-1 Protease flaps spontaneously open and reclose in molecular dynamics simulations. Proc. Natl. Acad. Sci. U.S.A 2006, 103, 915–920. [PubMed: 16418268]

(24). Quercia R; di Perri G; Pein C; Bodie J; Singh RSP; Hendrick V; Boffito M Ritonavir: 25 Years' Experience of Concomitant Medication Management. A Narrative Review. Infect. Dis. Ther 2024, 13 (5), 1005–1017. [PubMed: 38609668]

(25). Kempf DJ; Marsh KC; Denissen JF; McDonald E; Vasavanonda S; Flentge CA; Green BE; Fino L; Park CH; Kong XP ABT-538 Is a Potent Inhibitor of Human Immunodeficiency Virus Protease and Has High Oral Bioavailability in Humans. Proc. Natl. Acad. Sci. U.S.A 1995, 92 (7), 2484–2488. [PubMed: 7708670]

(26). Champenois K; Baras A; Choisy P; Ajana F; Melliez H; Bocket L; Yazdanpanah Y Lopinavir/ ritonavir resistance in patients infected with HIV-1: Two divergent resistance pathways? J Med Virol 2011, 83 (10), 1677–1681. [PubMed: 21755502]

(27). Shekhar M; Smith Z; Seeliger MA; Tiwary P Protein Flexibility and Dissociation Pathway Differentiation Can Explain Onset of Resistance Mutations in Kinases. Angew. Chem., Int. Ed 2022, 61 (28), No. e202200983.

(28). Ahmad K; Rizzi A; Capelli R; Mandelli D; Lyu W; Carloni P Enhanced-Sampling Simulations for the Estimation of Ligand Binding Kinetics: Current Status and Perspective. Front. Mol. Biosci 2022, 9, 899805. [PubMed: 35755817]

(29). Miao Y; Huang YM; Walker RC; McCammon JA; Chang CA Ligand Binding Pathways and Conformational Transitions of the HIV Protease. Biochemistry 2018, 57 (9), 1533–1541. [PubMed: 29394043]

(30). Doshi U; Hamelberg D Towards fast, rigorous and efficient conformational sampling of biomolecules: Advances in accelerated molecular dynamics. Biochim. Biophys. Acta, Gen. Subj 2015, 1850 (5), 878–888.

(31). Sun J; Raymundo M. A. v.; Chang CEA Ritonavir and xk263 Binding-Unbinding with HIV-1 Protease: Pathways, Energy and Comparison. Life 2022, 12 (1), 116. [PubMed: 35054509]

(32). Wang C; Greene D; Xiao L; Qi R; Luo R Recent Developments and Applications of the MMPBSA Method. Front. Mol. Biosci 2018, 4, 87. [PubMed: 29367919]

(33). Tang Z; Chen S-H; Chang CA Transient States and Barriers from Molecular Simulations and the Milestoning Theory: Kinetics in Ligand–Protein Recognition and Compound Design. J. Chem. Theory Comput 2020, 16 (3), 1882–1895. [PubMed: 32031801]

(34). Ruzmetov T; Montes R; Sun J; Chen SH; Tang Z; Chang CEA Binding Kinetics Toolkit for Analyzing Transient Molecular Conformations and Computing Free Energy Landscapes. J. Phys. Chem. A 2022, 126 (46), 8761–8770. [PubMed: 36346951]

(35). Elber R. A new paradigm for atomically detailed simulations of kinetics in biophysical systems. Q. Rev. Biophys 2017, 50, No. e8. [PubMed: 29233220]

(36). Lazim R; Suh D; Choi S Advances in Molecular Dynamics Simulations and Enhanced Sampling Methods for the Study of Protein Systems. Int. J. Mol. Sci 2020, 21 (17), 6339. [PubMed: 32882859]

(37). Huang YM; Kang M; Chang CA Switches of hydrogen bonds during ligand–protein association processes determine binding kinetics. J. Mol. Recognit 2014, 27 (9), 537–548. [PubMed: 25042708]

(38). Qu S; Huang S; Pan X; Yang L; Mei H Constructing Interconsistent, Reasonable, and Predictive Models for Both the Kinetic and Thermodynamic Properties of HIV-1 Protease Inhibitors. J. Chem. Inf. Model 2016, 56 (10), 2061–2068. [PubMed: 27624663]

(39). Chen J; Yang M; Hu G; Shi S; Yi C; Zhang Q Insights into the functional role of protonation states in the HIV-1 protease-BEA369 complex: molecular dynamics simulations and free energy calculations. J. Mol. Model 2009, 15 (10), 1245–1252. [PubMed: 19294437]

(40). Roe DR; Cheatham TE PTRAJ and CPPTRAJ: Software for Processing and Analysis of Molecular Dynamics Trajectory Data. J. Chem. Theory Comput 2013, 9 (7), 3084–3095. [PubMed: 26583988]

(41). Hung TI; Hsieh YJ; Lu WL; Wu KP; Chang C. en A. What Strengthens Protein-Protein Interactions: Analysis and Applications of Residue Correlation Networks. J. Mol. Biol 2023, 435 (24), 168337. [PubMed: 37918563]

(42). Limongelli V; Bonomi M; Parrinello M Funnel metadynamics as accurate binding free-energy method. Proc. Natl. Acad. Sci. U.S.A 2013, 110 (16), 6358–6363. [PubMed: 23553839]

(43). Ray D; Stone SE; Andricioaei I Markovian Weighted Ensemble Milestoning (M-WEM): Long-Time Kinetics from Short Trajectories. J. Chem. Theory Comput 2022, 18 (1), 79–95. [PubMed: 34910499]

(44). Tang Z; Chen S-H; Chang CA Transient States and Barriers from Molecular Simulations and the Milestoning Theory: Kinetics in Ligand–Protein Recognition and Compound Design. J. Chem. Theory Comput 2020, 16 (3), 1882–1895. [PubMed: 32031801]

(45). Whitfield TW; Ragland DA; Zeldovich KB; Schiffer CA Characterizing Protein-Ligand Binding Using Atomistic Simulation and Machine Learning: Application to Drug Resistance in HIV-1 Protease. J. Chem. Theory Comput 2020, 16 (2), 1284–1299. [PubMed: 31877249]
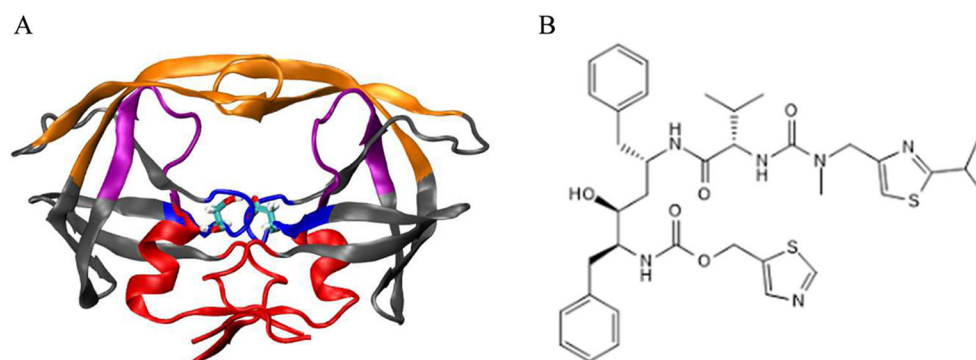
A

B

Figure 1.
HIVp and ritonavir structures. (A) HIVp structure with color-coded regions: flap (orange: residues 42–60 and 141–159), flap tips (orange: residues 49–52 and 148–151), loop (pink: residues 75–85 and 174–184), catalytic triads (blue: residues 23–29 and 122–128) and dimer interface (red: residues 1–9, 86–99, 100–108 and 185–198). Catalytic residues, Asp 25 and Asp 124, are shown in licorice. (B) Two-dimensional structure of HIVp inhibitor ritonavir.
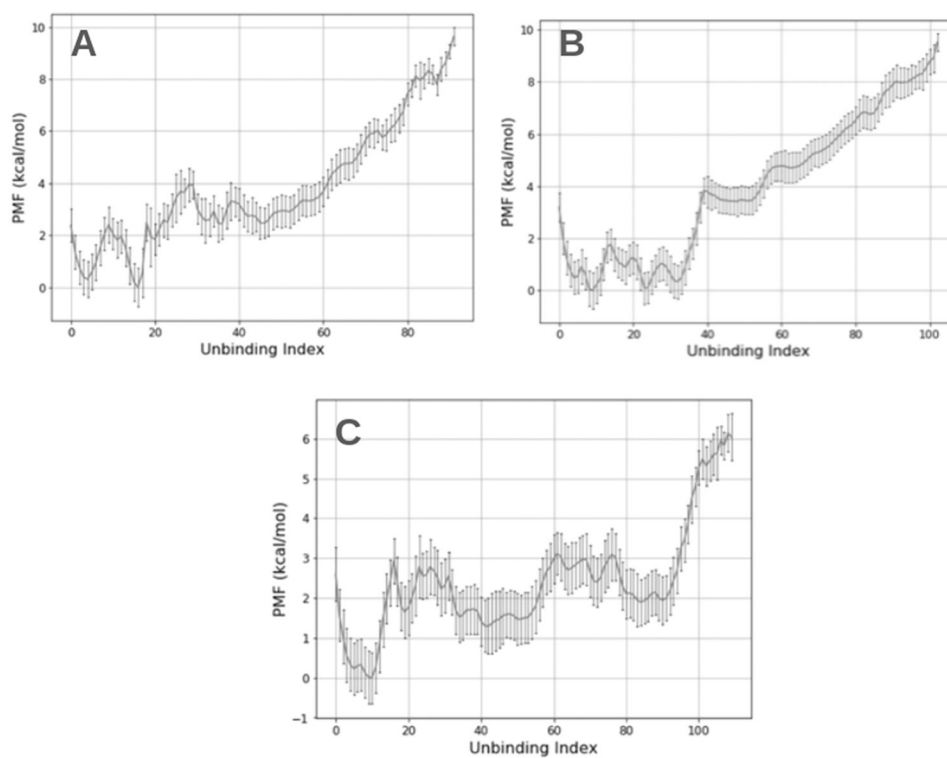
Figure 2.
Pathway specific free energy landscape of ritonavir unbinding from HIVp. Free energy landscape of pathway A (A), pathway B (B), and pathway C (C) computed using unbinding coordinates defined from the PC space, labeled as PC coordinate in Table 1. Pathways A and B demonstrate a progressive increase in energy. Pathway C exhibits an initial jump in energy, followed by a large plateau, before a final energy jump upon unbinding. The absolute binding free energy G estimated from the plots is systematically underestimated, compared with experimental results. However, the free energy plots allow for relative energy studies of local minima and maxima.
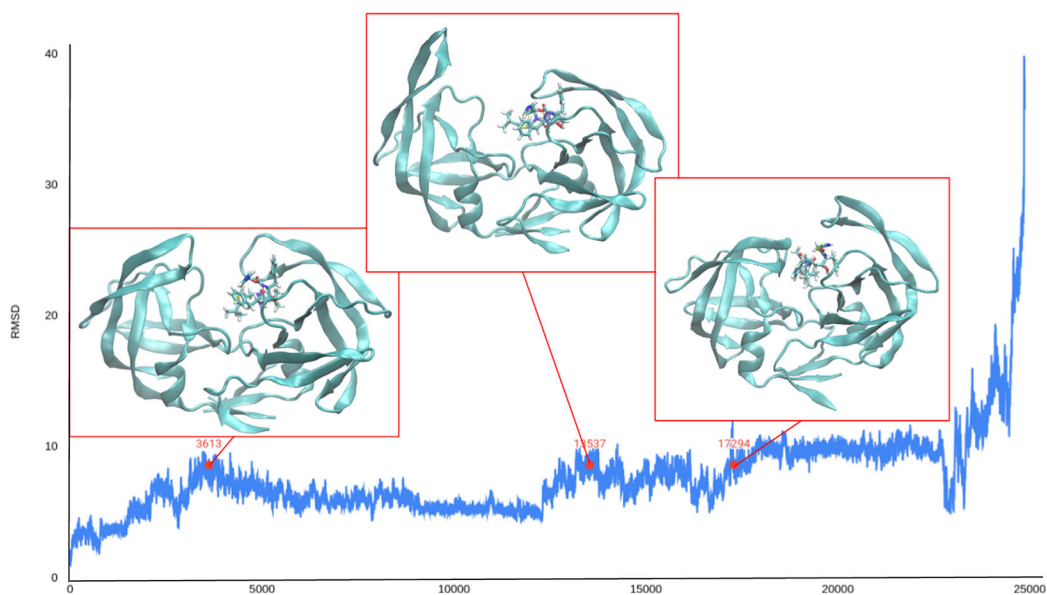
Figure 3.
Ritonavir rmsd during dissociation pathway A. Ritonavir rmsd is seen going up and down during dissociation, representing a back-and-forth motion in the pocket. This results in many frames having the same rmsd value. Ritonavir position is visualized for frames #3613, #13537, and #17294, where each frame was saved every 10 ps. These frames all have a rmsd value of 8.62 Å, yet represent different positioning, and occur at drastically different time points during the trajectory.
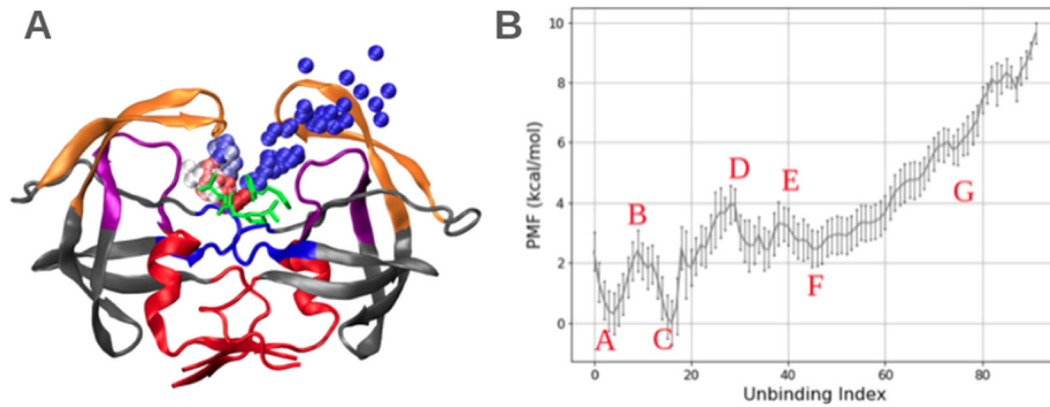
Figure 4.
Free energy landscape of ritonavir unbinding from HIVp under pathway A. (A) Ritonavir dissociation under pathway A. HIVp colored as in Figure 1. Each bead represents a position of center of mass of ritonavir with 1 ns interval taken from aMD dissociation, with total simulation time of 248.7 ns. The HIVp conformation is taken from the final frame of the dissociation trajectory. Color beads present center of mass of ritonavir taken from frames in the beginning (red), middle (white) and near the end (blue) of the trajectory. Ritonavir's initial position is green licorice. (B) Free energy landscape of ritonavir under pathway A with labeled maxima and minima. Ritonavir major energy barriers (B,D,E) and local minimum (A,C,F,G) labeled in red, and the conformations are detailed in Figure 5.
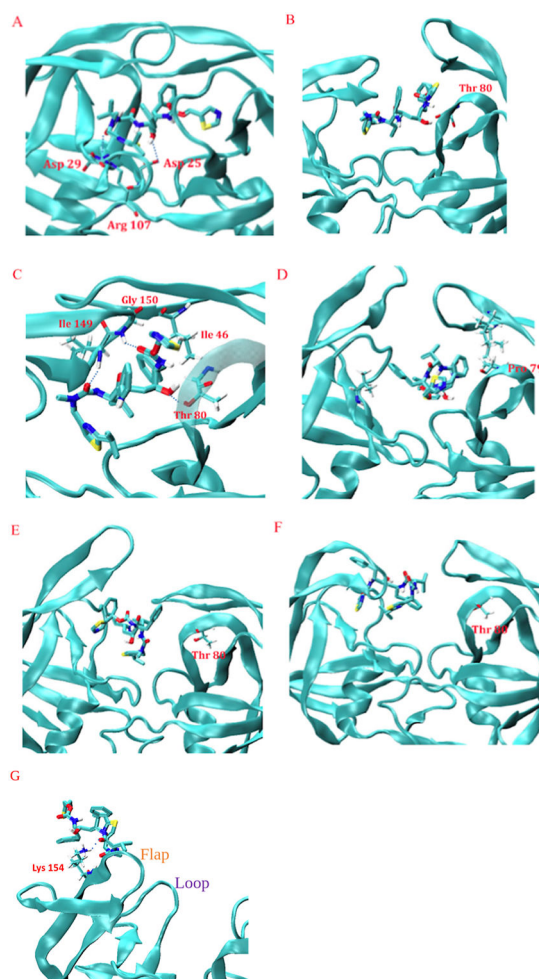
Figure 5.
Progression of molecular interactions of ritonavir and HIVp during dissociation via pathway A. A–G show local energy minima or barriers indicated in Figure 4. (A,C,G). Local free energy minima are explained via bound-state stabilization by hydrogen bonds between ritonavir and HIVp. (B,D,E) Free energy barriers are seen when these hydrogen bonds are broken, and ritonavir is positioned that allows high solvent exposure. (F) A free energy minimum reveals a favorable ritonavir positioning between the flap and loop regions.
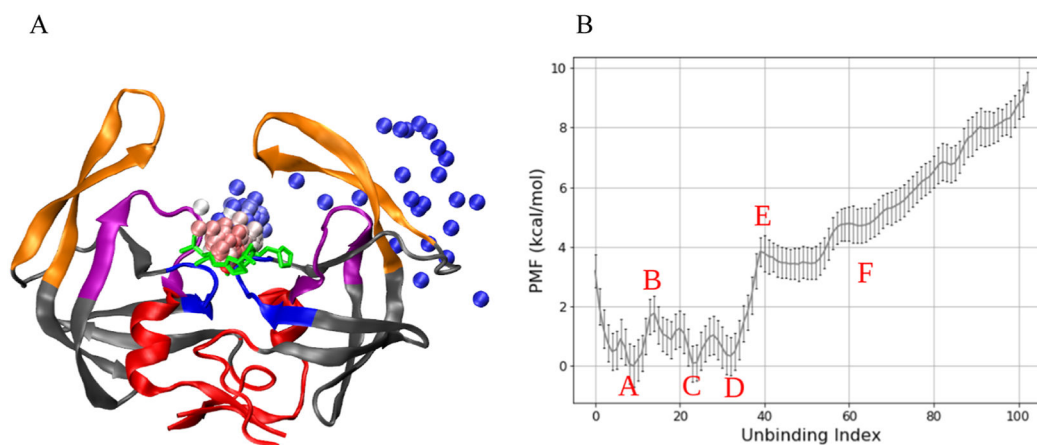
A

B

Figure 6.

Free energy landscape of ritonavir unbinding from HIVp under pathway B. (A) Ritonavir dissociation under pathway B. HIVp colored as in Figure 1. Each bead represents a position of center of mass of ritonavir with 1 ns interval taken from aMD dissociation, with total simulation time of 304.9 ns. The HIVp conformation is taken from the final frame of the dissociation trajectory. Color beads present center of mass of ritonavir taken from frames in the beginning (red), middle (white) and near the end (blue) of the trajectory. Ritonavir's initial position is green licorice. (B) Free energy landscape of ritonavir under pathway B with labeled maxima and minima. Major energy barriers (B,E) and local minimum (A,C,D,F) labeled in red, and the conformations are detailed in Figure 7.
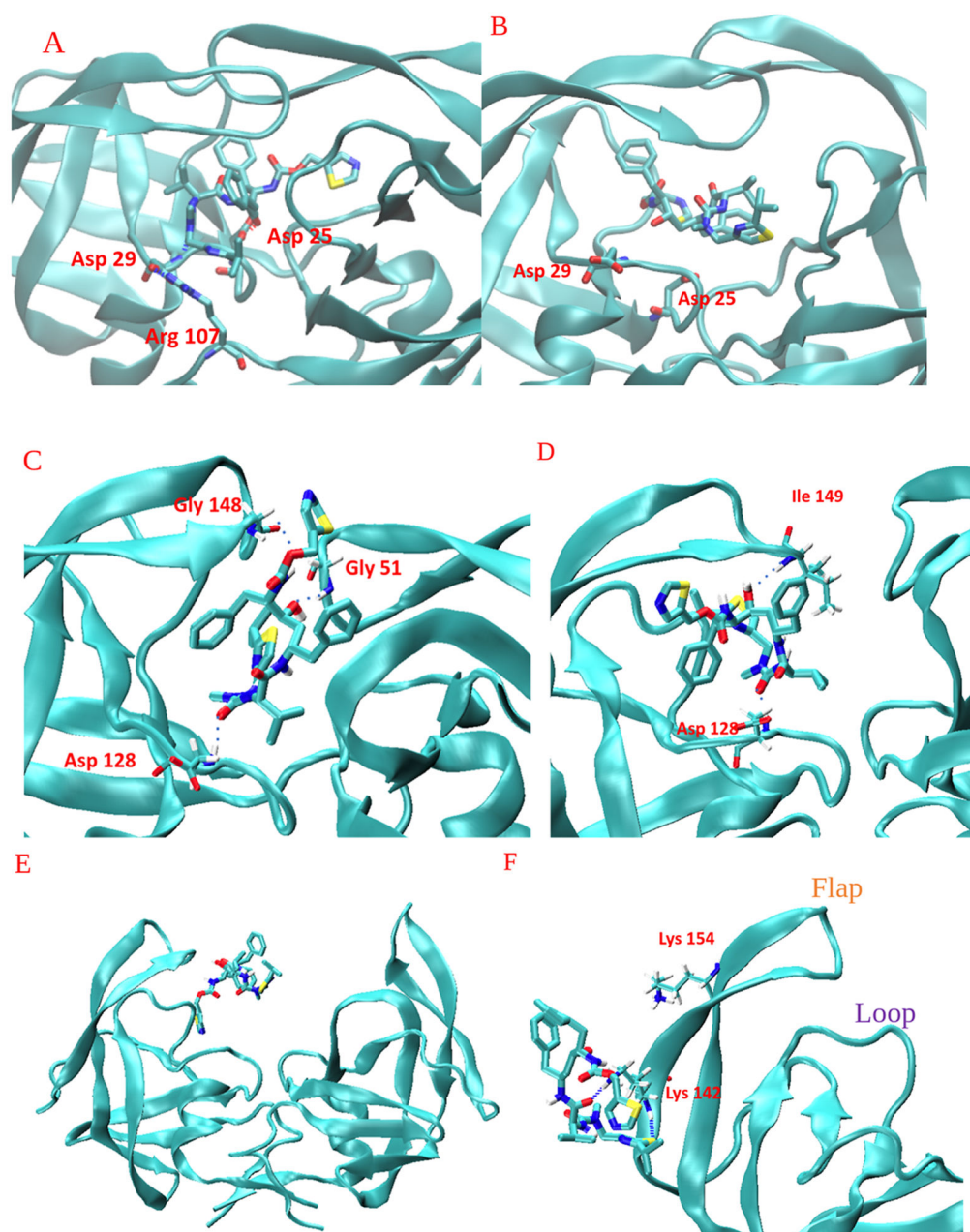
Figure 7.
Progression of molecular interactions of ritonavir and HIVp during dissociation via pathway B. Local energy minima or barriers are indicated in Figure 6. (A,C,D,F) Local energy energy minima are explained via bound-state stabilization by hydrogen bonds between ritonavir and HIVp. (B,E) Local free energy barrier has appeared when these bonds are broken, and ritonavir is positioned that allows high solvent exposure.
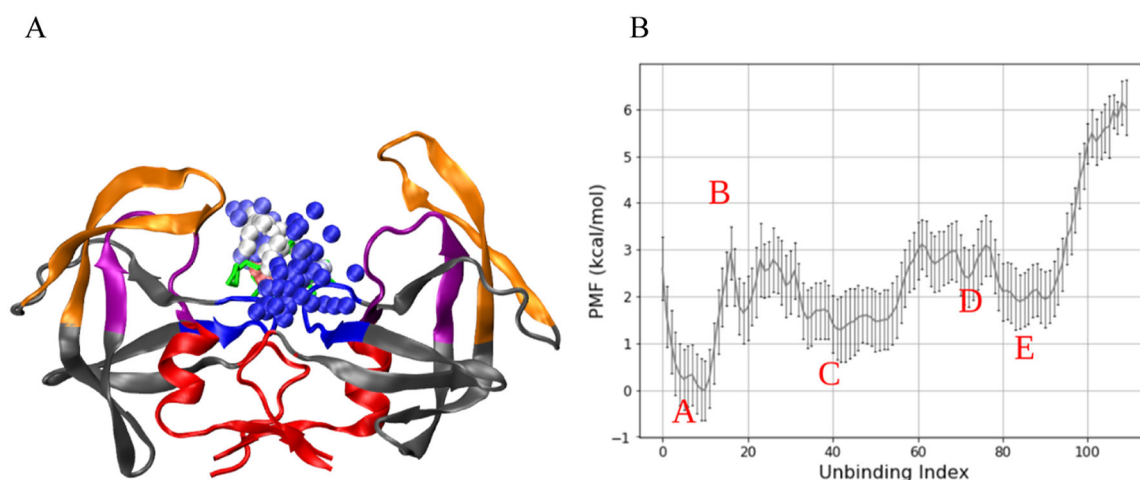
A

B

Figure 8.
Free energy landscape of ritonavir unbinding from HIVp under pathway C. (A) Ritonavir dissociation under pathway C. HIVp colored as in Figure 1. Each bead represents a position of center of mass of ritonavir with 1 ns interval taken from aMD dissociation, with total simulation time of 543.1 ns. The HIVp conformation is taken from the final frame of the dissociation trajectory. Color beads present center of mass of ritonavir taken from frames in the beginning (red), middle (white) and near the end (blue) of the trajectory. Ritonavir's initial position is green licorice. (B) Free energy landscape of ritonavir under pathway B with labeled maxima and minima. Major energy barriers (B) and local minimum (A,C,D,E) labeled in red, and the conformations are detailed in Figure 9.
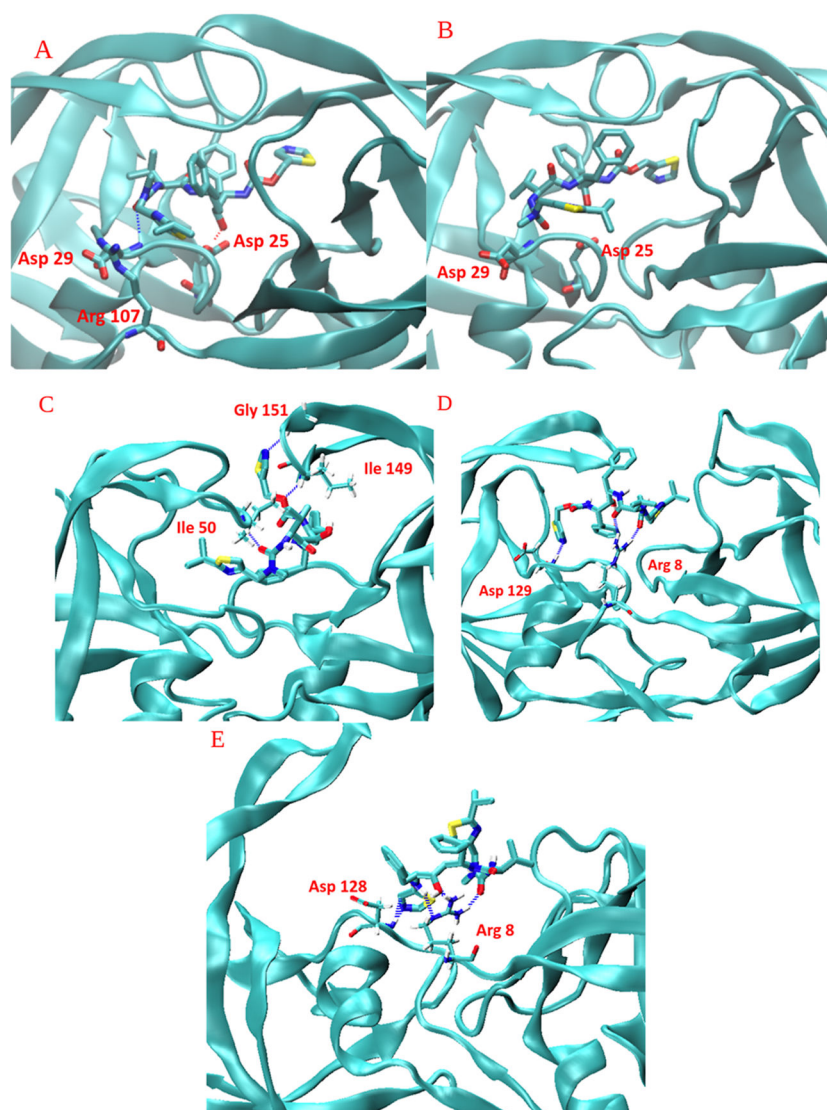
Figure 9.
Progression of molecular interactions of ritonavir and HIVp during dissociation via pathway C. Local energy minima or barriers are indicated in Figure 8. (A,C,D,E) Local free energy minima are explained via bound-state stabilization by hydrogen bonds between ritonavir and HIVp. (B) Free energy barrier can be described by the breaking of favorable interactions.
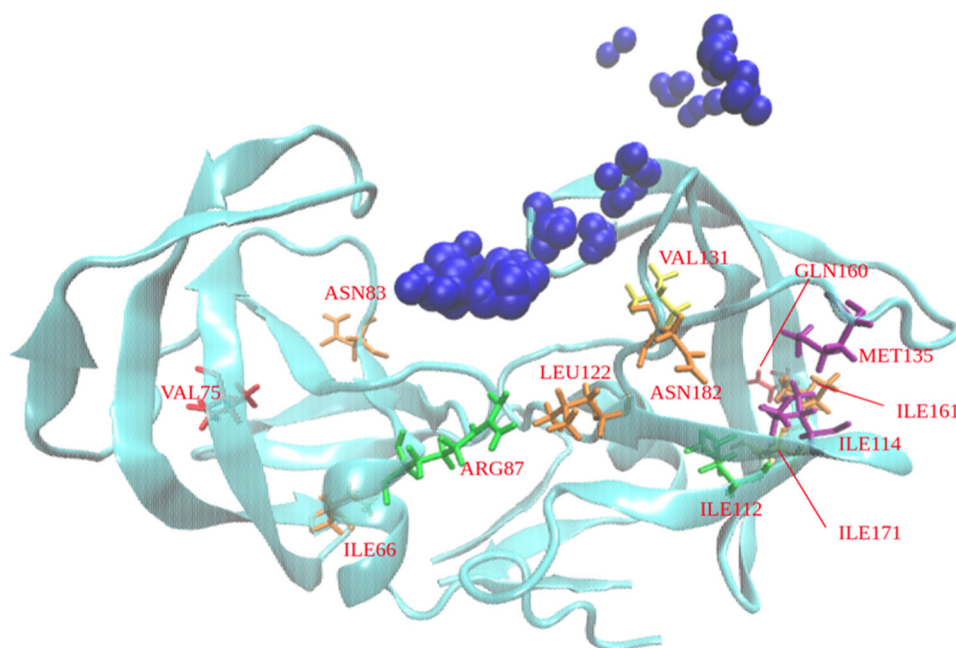
Figure 10.
Highly positively correlated residue in ritonavir–HIVp dissociation pathway A. HIVp shown in cyan. Ritonavir position during dissociation taken from representative frames shown in bead illustration (gray), dissociating between the flap and the loop regions. Crude approximate binding spheres are used to show general ritonavir location. Image captures backbone and side chain positions at the final unbinding index. Residues are dispersed in all regions excluding the flap regions. Increased number of correlated residues on side in which ritonavir dissociates. Side chain colors reflect correlation pairings/groups.
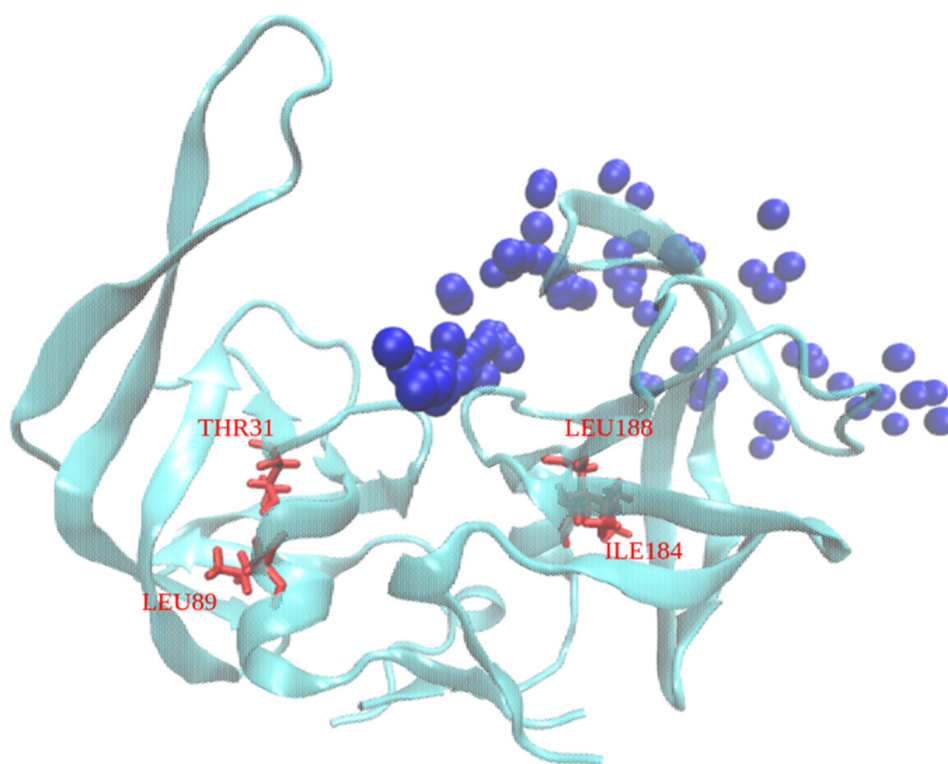
Figure 11.
Highly positively correlated residue in ritonavir–HIVp dissociation pathway B. HIVp shown in cyan. Ritonavir position during dissociation taken from representative frames shown in bead illustration (gray), dissociating along the flap region. Crude approximate binding spheres are used to show general ritonavir location. Image captures backbone and side chain positions at the final unbinding index. Correlated residues are primarily localized to the interface region and are absent from the flap region. Only one correlation group is present (red).
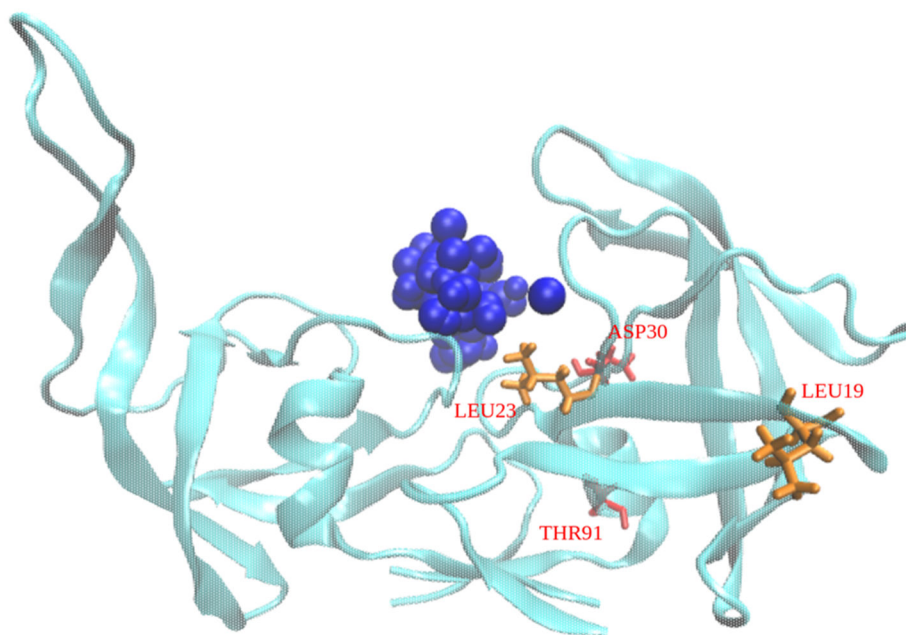
Figure 12.
Highly positively correlated residue in ritonavir–HIVp dissociation pathway C. HIVp shown in cyan. Ritonavir position during dissociation taken from representative frames shown in bead illustration (gray), dissociating on the interface region. Crude approximate binding spheres are used to show general ritonavir location. Image captures backbone and side chain positions at the final unbinding index. Side chain colors reflect correlation pairings/groups. Correlated residues show no distinct localization.

Table 1.

Calculated and Experimental Unbinding Free Energy Values and Pathway Occurrence[a]

	PC coordinate		rmsd coordinate		experimental		aMD
	binding free energy (ΔG)	residence time (μs)	binding free energy (ΔG)	residence time (s)	binding free energy (ΔG)	residence time (s)	occurrence (%)
pathway A	-9.4 ± 0.8	483 ± 219	-14.1 ± 0.5	2.5 ± 0.2	-13.7	463	55
pathway B	-9.5 ± 0.8	2010 ± 501	-15.4 ± 0.5	41.6 ± 3.8	-13.7	463	20
pathway C	-6.1 ± 0.8	4.5 ± 1.1	-14.9 ± 0.6	29.6 ± 2.3	-13.7	463	15

[a] Pathway-specific binding free energy (kcal/mol) and residence time computed with coordinates assigned using the PC space (labeled PC coordinate) and ligand rmsd (labeled rmsd coordinate) in comparison to experimental values. Percentages show frequency of each pathway out of a total of 20 successful ligand dissociation runs modeled by aMD simulations.[31] Percentages do not add up to 100% due to negation of undefined pathways.

Table 2.

Residues with Substantial Correlation in Ritonavir–HIVp Dissociation Pathway A[a]

positive correlation (>0.5)			negative correlation (←0.5)		
residue	residue	correlation	residue	residue	correlation
ILE66	ASN83	0.601541	TYR59	ASN83	−0.52429
VAL75	GLN160	0.529861	ILE62	TRP141	−0.51558
VAL82	GLN101	0.501499	ILE62	LEU122	−0.599
ASN83	ASN182	0.573296	ASN83	ASN182	−0.5665
ASN83	ILE161	0.530882	ASN83	ASN182	−0.6823
ASN83	ASN182	0.644101	ILE84	ILE165	−0.50422
ARG87	ILE112	0.526643	GLN92	ILE183	−0.51592
ILE114	MET135	0.508678	ILE112	ASN83	−0.56379
LEU122	ASN182	0.547785			
VAL131	ILE171	0.505891			

[a]Positive correlation cutoff >0.50. Negative correlation cutoff <–0.50. 10 residue pairs had significant positive correlation. 8 residue pairs had a significant negative correlation.

Table 3.

Residues with Substantial Correlation in Ritonavir–HIVp Dissociation Pathway B and Pathway C[a]

pathway	residue	residue	correlation
B	THR31	LEU89	0.523319
B	LEU89	ILE184	0.625443
B	ILE184	LEU188	0.654553
B	ILE183	LEU189	−0.50999
C	LEU19	LEU23	0.504406
C	ASP30	THR91	0.506992

[a]Positive correlation cutoff >0.50. Negative correlation cutoff <−0.50. Pathway B shows 3 residue pairs with significant positive correlation and 1 residue pair with a significant negative correlation. In pathway C, 2 residue pairs were identified with a significant positive correlation and 0 residues shared a significant negative correlation.